Engineering: Faculty Publications

Engineering

2012

Channel Dimension Constraints for Miniature Low Humidity PEM Fuel Cells

Denise A. McKahn
Smith College, dmckahn@smith.edu

Xizhu Zhao
Smith College

Recommended Citation

FuelCell2012-91504

CHANNEL DIMENSION CONSTRAINTS FOR MINIATURE LOW HUMIDITY PEM FUEL CELLS

Denise A. McKahn and Xizhu Zhao
Picker Engineering Program, Smith College, Northampton, MA, 01063
Contact e-mail: dmckahn@smith.edu

ABSTRACT

Numerous applications exist requiring power for small loads (<5W) with minimal mass operating in extreme ambient conditions. Making progress toward reducing stack mass, we investigate the influence of flow field channel depth and endplate compression on cell performance. The best performance was found at endplate compressions of 139 psi, cathode channel depths of 0.032 in and anode channel depths of 0.032 in. The maximum power mass-density achieved with these 4.84 cm^2 cells was 16.8 mW/g in a single cell stack. If deployed in a multicell stack, this same performance would translate to a power mass-density of 45.3 mW/g, nearing the performance of off-the-shelf lithium ion batteries (approximately 70 mW/g).

1 INTRODUCTION

While a significant body of work has investigated polymer electrolyte membrane (PEM) fuel cells for vehicular applications, these fuel cells have only recently been explored as viable power supplies for miniature applications, such as lightweight meteorological balloons [1] and unmanned aerial systems [2, 3]. Due to significant mass restrictions, these systems are often operated under extreme conditions with ambient temperatures and no humidification or reactant pre-treatment.

With respect to reactant distribution, miniature fuel cells have relatively narrow and shallow channels. Channels depths were found to be between 100-400 μm [4], as opposed to an order of 1000 μm seen with standard PEMFCs. These smaller channels cause accumulated liquid water to more readily occlude channels. The occurrence of cathode flooding typically not observed until higher current density operation will be more pronounced in miniature fuel cells, setting a lower constraint on the range of operable current densities [5] as well as a tradeoff between space constraints and water management [6]. Moreover, the Peclet numbers are not sufficient for liquid water detachment through convection [7], a serious limitation for air breathing fuel cells [5]. Limiting current densities have been documented for different membrane materials with a range between 1.05-1.8 A/cm^2. However, little effort has been placed on determining the minimal channel depth under dry conditions. Because channel depth impacts the flow field plate thickness and thus plate mass, it is a critical design variable for achieving maximal energy density.

Past studies have considered the design decisions involved in constructing a miniature PEM fuel cell system, specifically detailing the system architecture and cell materials choices [1]. To build on this work, we aim to further decrease cell mass by reducing the thickness of the anode and cathode flow field collector plates used to distribute gases to the gas diffusion layer (GDL), while maintaining adequate GDL compression without mechanical plate failures. Thus, the influence of cathode and anode channel depths are studied in this work alongside endplate compression as they relate to cell performance (overpotential).

Identifying an optimal GDL compression level for a given set of fuel cell materials is critical for maximizing cell performance. In compressing the GDL, there is a tradeoff between reducing ohmic losses associated with both bulk and contact resistances of the GDL versus maximizing GDL porosity for im-

proved fluid and gas transport in the GDL. As GDL compression increases, electrical resistance decreases [8] and transport resistance increases. Therefore, an optimal balance must be struck between these two transport related phenomena. The compression ratio of the GDL, quantified by the percent of through-plane GDL deformation, has been studied to identify a desirable compression ratio or compressive load applied to the cell endplates.

There are two main methods that have been employed to measure GDL compression: those that apply a measured pressure or force to the outside of the stack and rely on those measurements to infer what happens inside the stack [9, 10], as opposed to those methods that directly measure pressure distribution in-situ [1, 11]. Each method has inherent constraints and assumptions that impact the application of the experimental results. For example, use of compression load cells, or pistons to measure the pressure or force applied to the endplate does not enable a direct measure of GDL compression due to the use of face seals (gaskets) that have significant elasticity. Additionally, the relationship between applied pressure and GDL compression ratio or deformation is nonlinear [12]. Therefore, one can not be easily inferred without characterizing each individual material. In-situ pressure distribution measurements, on the otherhand, are often made with pressure sensitive films that change color intensity as a function of applied pressure. Cells can not be operated with these films installed. Therefore, a relationship must be made between the torque applied to the tie-rods and the pressure sensed on this film for each given stack design, in order to relate clamping pressure to cell performance. Both methods should be used with caution when further estimating the fraction of the GDL that is actually compressed. With any of these methods each new material combination and stack design must be explored when determining the optimal clamping pressure.

A GORE PRIMEA 50 series MEA with ELATs and CARBEL Toray paper was explored by [13] at torques of 100-150 in-lb/bolt. Nafion 117 with Toray carbon paper were explored by [10] and Nafion 212 with SAATI carbon cloth substrates and varying microporous layer hydrophobicity were deployed using impedance spectroscopy to show that membrane resistance significantly decreases at the less significant cost of increased diffusion resistance [14]. While no direct measurements were taken of either pressure or force, the following authors tested the relationship between an estimated compression level and measured performance for different material combinations [9,15,16]. More specifically, Nafion 115 MEAs were used with ELATs and Toray Carbon paper by [15], Nan-Ya series bMEA5 with SGL 10BA and SGL 10AA with varying PTFE content were explored by [9], and Gore PRIMEA 57 series MEA with SGL 10BC were evaluated by [16].

In this work we carefully control the force applied to the fuel cell endplates and compare fuel cell performance with Nafion 212 and SGL 10BC under dry conditions at low temperature, providing data for a set of materials and operating conditions not yet evaluated in literature.

2 EXPERIMENTS

This section presents the experimental hardware used, specifically detailing the stack materials, the sizing of the gas channels, and the test bench setup.

2.1 Stack Materials

Each cell was comprised of a conductive and relatively impervious flow field separator/collector plate, Buna-N gaskets, gas diffusion layers (GDL), and a membrane electrode assembly (MEA). Endplates were used to apply a compressive force to the cells using tie-rods. Choices made in material selection and design are detailed in [1]. A summary table of the component masses is provided in Table 1, with a total single cell stack mass of 48.00 g.

TABLE 1. Cell component masses.

Part	Mass (g)
Cathode and Anode Graphite Flow Fields	20.52
Buna-N Gaskets	2.54
Acrylic Endplates	20.96
Plastic Fittings	1.88
Plastic Tie-rods and nuts	1.69
GDLs and MEA	0.41
Total single cell stack mass	48.00

The fuel cell utilizes standard commercially available MEAs purchased from Ion Power. These MEAs were either Nafion 211 or 212 membrane electrode assemblies, an active area of 4.84 cm^2, a catalyst layer of 0.3 mg/cm^2 Pt/C on the anode and cathode with no integrated gaskets. A non-woven SGL Sigracet 10BC GDL was chosen with an uncompressed thickness of 0.38 mm.

Four tie-rods were used to hold the cell materials together and tightened sufficiently to avoid material displacement on handling. Stack compression was then maintained using an Instron, as described in Section 3.1. To reduce weight, acrylic endplates were selected along with PTFE tie-rods and bolts.

The anode and cathode flow fields were made of 3.18 mm GM10 grade Graphtek graphite blanks. Straight channels were employed on both the anode and cathode flow fields. Each channel was machined to a width of 1.17 mm with the channel lands and grooves evenly spaced and parallel. The internal manifolds
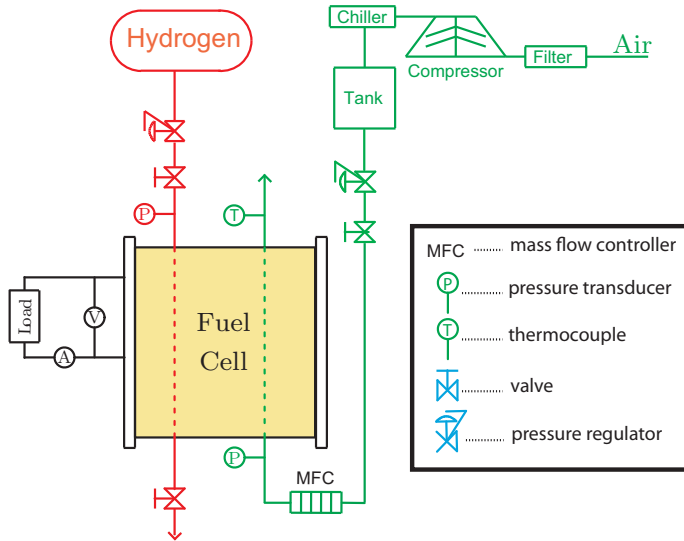
FIGURE 1. Fuel cell experimental hardware.

used to distribute gas between cells were located at the entrance and exit of each of the channels.

2.2 Hardware

A detailed analysis of the system architecture used for miniature fuel cells in ambient applications is provided in [1]. The fuel cell operates with no reactant pre-treatment (humidification), a dead ended and pressure controlled anode, and a flow controlled cathode. A schematic of the major system components is depicted in Figure 1, specifically targeting experimentation not deployment. When the fuel cell is deployed, the air compressor, air storage tank and mass flow controller would be replaced with a miniature air pump.

Dry pure hydrogen is pressure regulated at the anode inlet to 1.8 psig (1.14 bar). This pressure regulation system replenishes the hydrogen consumed in the chemical reaction. Thus, presuming the stack does not contain a leak, the hydrogen mass flow rate is equal to the reaction rate. For the majority of the operational time, the hydrogen stream is dead-ended with no flow external to the anode. Using a purge valve located downstream of the anode, hydrogen can be momentarily purged through the anode to remove water and gases that may accumulate at the anode as a result of membrane cross-over.

The mass flow rate of dry air is provided to the cathode at either a stoichiometric ratio or at a fixed mass flow rate. A stream of dry, oil-less air is supplied to the cathode using a mass flow controller. The cathode is operated as flow through, implying that the cathode exhaust gases are vented.

No cooling equipment is used with the miniature fuel cells in this work. The amount of heat generated due to the chemical reaction is not sufficient to increase the cathode outlet tem-

perature above 32 ^{o}C in a room with an ambient temperature of 25 ^{o}C. Should the active area be substantially larger, or a substantial number of cells be added to the stack, the need for cooling should be reassessed.

The electronic load consists of a variable potentiometer. Thus, the cell is operated in constant resistance mode. Note, this is distinctly different than operating the cell in galvanostatic mode which is often recommended for experimental work if variable contact resistance is expected at the GDL to gas channel (current collector) interface [17]. Prescale pressure paper was used to confirm relatively uniform compression across the active area. The decision to operate with constant (and controllable) resistance was made to mimic the type of load the fuel cell is expected to operate when deployed.

Several measurements are taken including total pressure, temperature, cell voltage and stack current. The locations of these sensors are indicated in Figure 1. In the gas plumbing external to the fuel cell stack the anode inlet and the cathode inlet total pressures are measured. Inside the fuel cell stack in the cathode exhaust manifold, the cathode outlet temperature is measured. The stack current is monitored with a current shunt. These measurements are acquired using off-the-shelf data acquisition and signal conditioning equipment. Specifically, signals are amplified using 5B Series signal conditioning modules with a 4Hz filter. Signals are acquired using a National Instruments USB-6212 multifunction data acquisition board and processed using LabVIEW.

2.3 Testing Protocol

Each fuel cell stack was tested under similar conditions and compared at the same point in membrane life. A testing protocol was established as shown in Figure 2. Each stack was operated at approximately 60 mA/cm^2 and 40 sccm air for just over an hour. A polarization curve was then taken. The stack continued to run for an additional 15 minutes at approximately 80 mA/cm^2 and another polarization curve was taken. The air mass flow rate was then increased to 100 sccm and the current density was increased to 140 mA/cm^2 for approximately 15 minutes. A polarization curve was then taken. The current density was increased to 200 mA/cm^2 for an additional 15 minutes followed be a second polarization curve at this air mass flow rate. The air mass flow rate was then further increased to 300 sccm, decreased to 100 sccm, then decreased to 40 sccm with polarization curves taken after 10-15 minutes of operation at each air mass flow rate.

To directly control and measure the clamping pressure applied to the endplates, each fuel cell stack was placed under a compressive load using an Instron 5542 Electromechanical Test Instrument with a 500 N frame. Steel block standoffs with a contact area of 0.797 in^2, centered on the active area, were used to transfer this load to the fuel cell endplates, resulting in applied pressures of up to 139 psi.
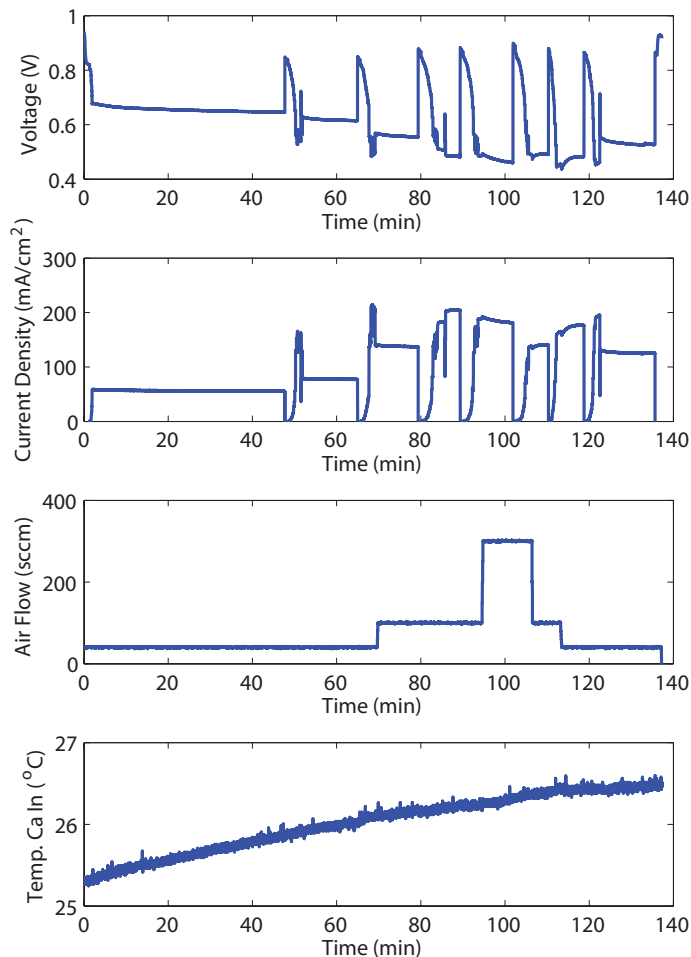
FIGURE 2. Dynamic experimental results for stack operating with Nafion 212, Sigracet 10BC, 0.046" deep channels on the cathode and anode. The subplots display stack voltage, current density, air mass flow rate, and cathode inlet temperature.

The cathode inlet and outlet temperatures are not constant throughout each experiment. The cathode inlet temperature is influenced by the air intake temperature and compressor conditions and is therefore not constant. However, there is little variation in the cathode inlet temperature, which remains between 23-27 ^{o}C throughout all experiments. As expected, the cathode outlet temperature is influenced by stack heat production and removal. An increase in the cathode air mass flow rate increases the heat removal rate and decreases the cathode outlet temperature. An increase in the stack current density results in an increase in cathode outlet temperature. Throughout the experiments, the cathode outlet temperature remains between 23-35°C.

It is important to note that the stack temperature (cathode outlet temperature) is relatively low for an operating PEM fuel cell, at approximately 30 ^{o}C as opposed to 60-80 ^{o}C common for

active areas greater than 100 cm^2. At these lower temperatures, it is expected that liquid water flooding could be more pronounced due to the decreased amount of water that can be entrained in the exhaust gases. However, the relatively low current density and the lack of supply gas humidification may result in less flooding than typically expected for low temperature PEM fuel cells.

3   RESULTS AND DISCUSSION

Results are presented and discussed in this section, specifically addressing the influence of GDL compression, cathode channel depth, and anode channel depth on the cell polarization performance with dry reactant supply gases.

3.1   GDL Compression Results

A stack was operated as described in Section 2.3 for the first hour of operation at a fixed air mass flow rate. A sequence of polarization curves was then taken, at three clamping pressures ranging between 100-139 psi . Figure 3 compares the influence of clamping pressure on cell polarization.
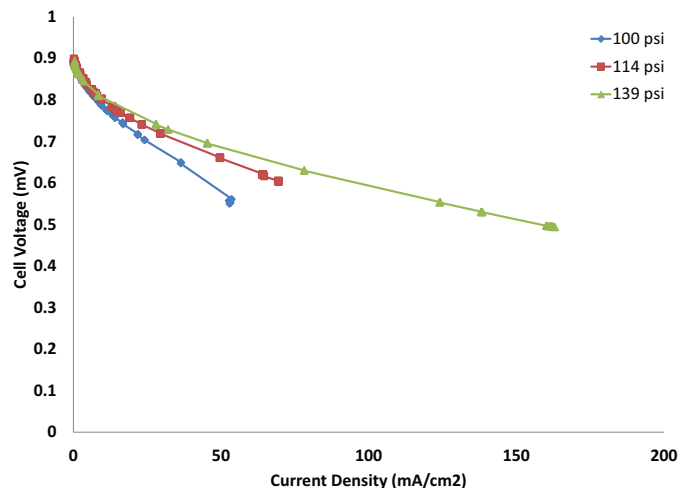

FIGURE 3. Influence of gas diffusion layer compression on performance. Polarization curves taken at a fixed cathode mass flow rate of 40sccm, a cathode outlet temperature of approximately 30°C, and dry reactant gas supply streams. The stack was comprised of Nafion 212 and SGL Sigracet 10BC gas diffusion layers.

As expected, increasing clamping pressure improves cell polarization by clearly reducing ohmic losses, with little impact on activation losses. The most significant decrease in ohmic losses occurs when increasing clamping pressure from 100 psi to 114 psi. A less appreciable decrease in ohmic losses occurs when increasing clamping pressure from 114 psi to 139 psi. While

Copyright © 2012 by ASME

139 psi results in the best performance, it is important to note that higher compression levels were not tested. Thus, an optimal compressive load was not determined. That said, we suspect that we were nearing or surpassing the optimal compression level due to the relatively small improvement in performance observed between 114 psi and 139 psi.

As mentioned previously, there is a tradeoff between increasing transport resistance in order to decrease electrical resistance as the compressive load increases. Electrode flooding, typically seen at high current densities, further exacerbates transport resistance. An optimal clamping pressure of 112 psi was found by [18] for SGL 10BB and 39 psi for SGL 10BA (no microporous layer) at 110 mA/cm^2. As expected, at the low humidity conditions of interest in this work, the compression level resulting in the best performance is greater than that found by [18] for similar materials.

3.2 Anode Channel Depth Results

The influence of the anode channel depth was assessed while varying the air mass flow rates with a cathode channel width and depth of 0.046 in and an anode channel width of 0.046 in. Cells were constructed with a Nafion 211 MEA and SGL 10BC GDL. The applied clamping pressure was approximately 100 psi. The results of these tests are shown in Figure 4.

For all air mass flow rates and current densities tested, the anode channel depth resulting in the best performance is the shallowest channel depth tested, namely 0.032 in. Interestingly, the cell polarization at different anode channel depths is a function of the cathode air mass flow rate. As the air mass flow rate supplied to the cathode increases from 40 to 300 sccm, the improvement in performance seen with shallower anode channels becomes less appreciable, with very little difference between the 0.032 in and 0.046 in deep channels.

The open circuit voltages are not appreciably influenced by cathode air mass flow rate. This is thought to be due to the relatively high hydrogen crossover expected with thin membranes (Nafion 211) dominating the influence of the increased oxygen partial pressures at higher air mass flow rates.

The ohmic losses result in the most significant difference in cell polarization at varying anode channel depths and air mass flow rates. The operating conditions that influence ohmic losses are membrane water content, temperature and oxygen partial pressure, whereas the design variable here that influences ohmic losses is the bulk electrical resistance. As the channel depth decreases, the in-plane electrical resistance decreases (shorter path to the electrical cable), with an anticipated decrease in the ohmic loss and thus improvement in cell performance. It is important to note that this bulk electrical resistance improvement is fixed (not a function of operating conditions). Thus, it is not surprising that the shallowest anode channel depth results in the best cell polarization.
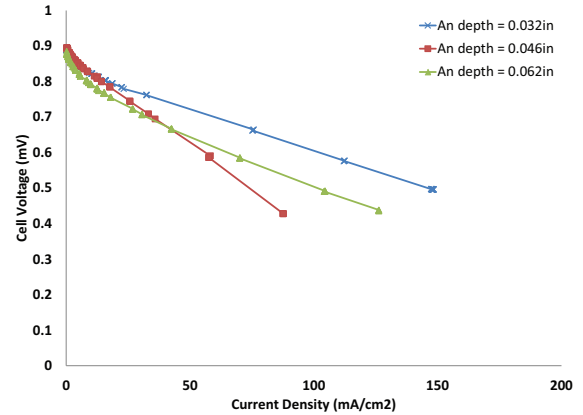
(a) Polarization curve taken at a fixed cathode mass flow rate of 40sccm.
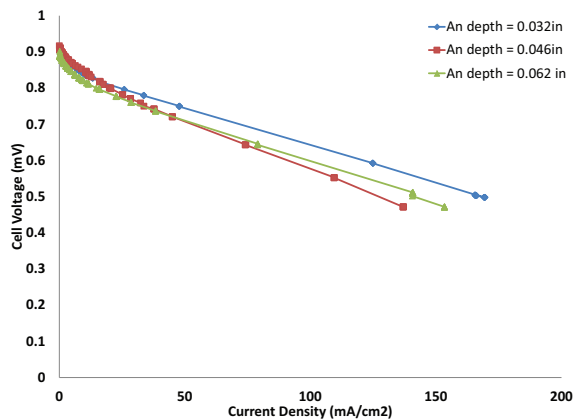
(b) Polarization curve taken at a fixed cathode mass flow rate of 100sccm.
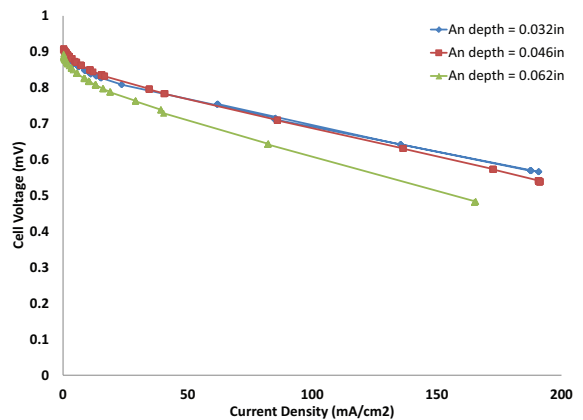
(c) Polarization curve taken at a fixed cathode mass flow rate of 300sccm.

FIGURE 4. Influence of anode channel depth on performance at different fixed air mass flow rates, 30°C and dry reactant supply gases. The cells are constructed using a Nafion 211 MEA and SGL 10BC GDL.

What is surprising, is that the best cell performance for the other two anode channel depths changes as a function of air mass flow rate. Interestingly, the membrane water content, oxygen partial pressure and cell temperature are all influenced by the cathode air mass flow rate. Due to back diffusion of gases from the cathode to the anode, these variables also influence the hydrogen partial pressure at the anode, in turn related to the anode channel depth. Generally, as air mass flow rate increases, the cell temperature decreases, causing an increase in the ohmic losses and degrading cell polarization. Additionally, an increase in the air mass flow rate for a given current density will decrease membrane water content and, thus, cell polarization. However, an increase in air mass flow rate will increase oxygen partial pressure, which improves cell polarization. Interestingly, the deviations in performance associated with anode channel depth are most pronounced at the lowest air mass flow rate. A more thorough investigation into the influence of these operating conditions is therefore warranted to elucidate the exact mechanisms resulting in the performance observed.

At a given current density, lower air mass flow rates result in lower air stoichiometries and air velocities. Any liquid water that may accumulate in the gas channels under these conditions would be less likely to be entrained in the gas stream and removed from the cell. To assess whether liquid water accumulation occurred, the cells were periodically surged with air, resulting in a rapid but unsustained increase in cell voltage due to the increased oxygen partial pressures. As a result, it is assumed that the cells are not operating under flooded cathode conditions in these tests. While anode flooding typically dominates at low current density in stacks with well humidified cathodes [19, 20], the anode is not expected to be flooded at low current density when the cathode is operated under dry conditions.
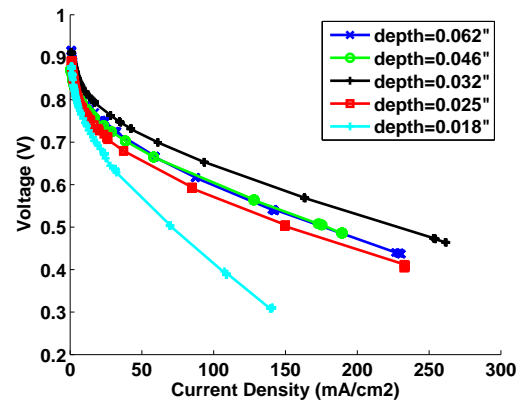
3.3 Cathode Channel Depth Results

The influence of the cathode channel depth was assessed with an anode channel width and depth of 0.046 in and a cathode channel width of 0.046 in. In these tests, cells were constructed with a Nafion 212 MEAs and SGL 10BC GDL. The applied clamping pressure was 139 psi, larger than that tested for the variable anode channel depth. The results of these tests are shown in Figure 5. Unlike with the anode, the cell polarization resulting in the best performance is a function of the air mass flow rate.

At 40 sccm, the cell polarization improves as cathode channel depth increases, with the performance of the deepest cathode channels showing the greatest performance. At current densities greater than 200 mA/cm^2, at an air mass flow rate of 40 sccm, the cell polarization is not statistically significantly different between 0.062 in and 0.046 in cathode channel depths or between 0.032 in, 0.025 in and 0.018 in. At both 100 sccm and 300 sccm air mass flow rates, cathode channel depths of 0.032 in result in
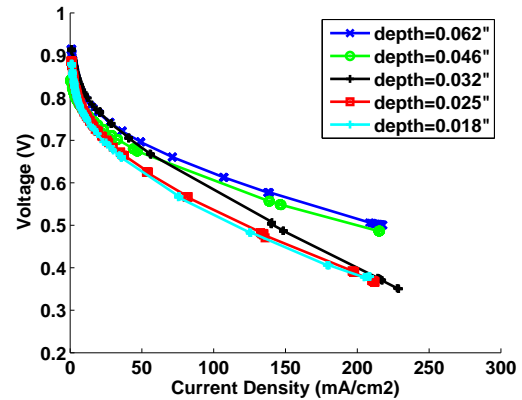
(a) Polarization curve taken at a fixed cathode mass flow rate of 40sccm.

(b) Polarization curve taken at a fixed cathode mass flow rate of 100sccm.
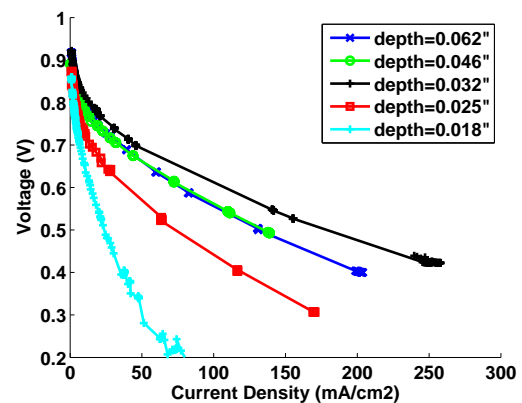
(c) Polarization curve taken at a fixed cathode mass flow rate of 300sccm.

FIGURE 5. Influence of cathode channel depth on performance at different fixed air mass flow rates, 30°C and dry reactant supply gases. The cells are constructed using a Nafion 212 MEA and SGL 10BC GDL.

Copyright © 2012 by ASME

the best performance, again with little difference in performance between channels depths of 0.062 in and 0.046 in.

Interestingly, as the air mass flow rate increases, the shallow channel depths appreciably degrade in performance in both the activation and ohmic regions of the polarization curves. As the cathode channel depth increases, the channel cross sectional area increases. When operating under fixed air mass flow rates, this increased channel cross sectional area results in lower air velocities and oxygen partial pressures at a given current density. As discussed with varying the anode channel depth, in these tests it is not expected that either anode or cathode flooding occurs due to the dry reactant gases supplied. Thus, it was expected that shallower cathode channels would result in reduced activation losses (greater oxygen partial pressures), which was counter to that observed.

The ohmic losses are a function of the membrane humidity, bulk and contact resistances, presuming that the cell temperature is relatively constant. For a given cathode channel depth, the contact and bulk electrical resistance should not be a function of air mass flow rate. Thus, any sensitivity to air mass flow rate indicates that membrane humidity might be the driving factor influencing the differences in ohmic losses observed at high flow. For a given channel depth, as air mass flow rate increases, the membrane humidity decreases and ohmic losses increase. As with the anode channel depth, it is also expected that increased cathode channel depths result in increased bulk ohmic resistance. Thus, the ohmic slope is not fixed from one cathode channel depth to the next, as shown.

Due to the range of current densities of interest, the stack will operate at air mass flow rates between 50-240 sccm/cell, with the most significant amount of time spent at higher flow. As a result, the recommended cathode channel depth is 0.032 in.

3.4 Overall Performance

The maximum sustained performance achieved was 16.8 mW/g for a stack employing Nafion 212, a cathode channel depth of 0.046" and an anode channel depth of 0.046". A channel depth of 0.032" on both the anode and cathode was not tested. However, the results presented in Section 3.3 suggest that this combination of gas channel depths will be superior in performance.

It is important to note that the test results presented here were for a single cell that was designed to be deployed in a multicell stack [1]. In a multicell stack, the flow fields in this design can be incorporated into bipolar plates, reducing the required number of flow field plates nearly in half. Additionally, some materials are only used in the stack in one location, like the endplates and gas fittings. Thus, the power mass-density increases as more cells are added to the stack given the same performance.

At the maximum power mass-density achieved, 16.8 mW/g, 6 cells would be needed in a stack to obtain the required 3.7VDC comparable to an off-the-shelf lithium ion battery. This 6 cell stack would include the same endplates, fittings, tie-rods and nuts, 6 MEAs and sets of GDL, 7 graphite flow fields, 2 endplate gaskets and 12 cell gaskets. The power mass-density of this 6-cell stack would therefore be expected to be 45.3 mW/g. While this power mass-density is still less than that seen with lithium ion batteries (70 mW/g), and does not include the mass of hydrogen and subsystems, a 35% improvement in performance or reduction in mass would, nonetheless, place these two technologies as direct competitors.

Currently the collector plates (flow fields) have a plate thickness of 0.125". Past testing has indicated that under compressive forces of 85 psi, approximately 0.020" of POCO TM grade graphite material should be maintained between the gas channels on each face of a bipolar plate. Thus, with channel depths of 0.032", this plate thickness could be reduced to 0.084" (a 33% decrease in thickness). Presuming that performance does not change with thinner plates, which is a very conservative assumption, the expected power mass-density would then be at least 56.8 mW/g.

4 CONCLUSIONS

The compressive force applied to the fuel cell endplates was explored, finding the best performance at 139 psi when using SGL Sigracet 10BC. Cathode and anode channel depths were also evaluated with fixed channel widths, finding the best performance using anode and cathode channel depths of 0.032 in. The maximum power mass-density achieved with these 4.84 cm^2 cells was 16.8 mW/g in a single cell stack. If deployed in a multicell stack, this same performance would translate to a power mass-density of 45.3 mW/g. If the flow field collector plate thickness were further reduced to an amount feasible with the relatively shallow 0.032 in channels, these cells would achieve a performance of 56.8 mW/g, nearing the performance of off-the-shelf lithium ion batteries (70 mW/g).

5 ACKNOWLEDGEMENTS

REFERENCES

[1] McKahn, D., and McMackin, W., 2011. "Characterizing performance of a pem fuel cell for a cmet balloon". In Proceedings of the ASME 9th International Conference on Fuel Cell Science, Engineering and Technology, ESFuelCell2011-54532.

[2] Bradley, T., Moffitt, B., Mavris, D., and Parekh, D., 2007. "Development and experimental characterization of a fuel

cell powered aircraft". *Journal of Power Sources, 171*, pp. 793–801.

[3] Kim, K., Kim, T., Lee, K., and Kwon, S., 2011. "Fuel cell system with sodium borohydride as hydrogen source for unmanned aerial vehicles". *Journal of Power Sources, 199*, pp. 9069–9075.

[4] Kundu, A., Jang, J., Gil, J., Jung, C., Lee, H., Kim, S.-H., Ku, B., and Oh, Y., 2007. "Micro-fuel cells - current development and applications". *Journal of Power Sources, 170*.

[5] Seyfang, B., Boillat, P., Simmen, F., Hartmann, S., Frei, G., Lippert, T., Scherer, G., and Wokaun, A., 2010. "Identification of liquid water constraints in micro polymer electrolyte fuel cells without gas diffusion layers". *Electrochimica Acta, 55*.

[6] Nguyen, N.-T., and Chan, S., 2006. "Micromachined polymer electrolyte membrane and direct methanol fuel cells - a review". *Journal of Micromechanics and Microengineering, 16*.

[7] Kumbur, E., Sharp, K., and Mench, M., 2006. "Liquid droplet behaviour and instability in a polymer electrolyte fuel cell flow channel". *Journal of Power Sources, 161*.

[8] Lin, J., Chen, W., Su, Y., and Ko, T., 2008. "Effect of gas diffusion layer compression on the performance in a proton exchange membrane fuel cell". *Fuel, 87*, pp. 2420–2424.

[9] Chang, H., Lin, C., Chang, M., Shiu, H., Chang, W., and Tsau, F., 2011. "Optimization of polytetrafluoroethylene content in cathode gas diffusion layer by the evaluation of compression effect on the performance of a proton exchange membrane fuel cell". *Journal of Power Sources, 196*, pp. 3773–3780.

[10] Canut, J. L., Latham, R., Merida, W., and Harrington, D., 2009. "Impedance study of membrane dehydration and compression in proton exchange membrane fuel cells". *Journal of Power Sources, 192*, pp. 457–466.

[11] Wang, X., Song, Y., and Zhang, B., 2008. "Experimental study on clamping pressure distribution in pem fuel cells". *Journal of Power Sources, 179*, pp. 305–309.

[12] Zhou, Y., Lin, G., Shih, A., and Hu, S., 2009. "Multiphysics modeling of assembly pressure effects on proton exchange membrane fuel cell performance". *Journal of Fuel Cell Science and Technology, 6*, pp. 041005–1 to 041005–7.

[13] Lee, W., Ho, C., Zee, J. V., and Murthy, M., 1999. "The effects of compression and gas diffusion layers on the performance of a pem fuel cell". *Journal of Power Sources, 84*, pp. 45–51.

[14] Dotelli, G., Omati, L., Stampino, P., Grassini, P., and Brivio, D., 2011. "Invesigation of gas diffusion layer compression by electrochemical impedance spectroscopy on running polymer electrolyte membrane fuel cells". *Journal of Power Sources, 196*, pp. 8955–8966.

[15] Ge, J., Higier, A., and Liu, H., 2006. "Effect of gas dif-

fusion layer compression on pem fuel cell performance". *Journal of Power Sources, 159*, pp. 922–927.

[16] Yim, S., Kim, B., Sohn, Y., Yoon, Y., Park, G., Lee, W., Kim, C., and Kim, Y., 2010. "The influence of stack clamping pressure on the performance of pem fuel cell stack". *Current Applied Physics, 10*, pp. S59–S61.

[17] Natarajan, D., and Nguyen, T., 2004. "Effect of electrode configuration and electronic conductivity on current density distribution measurements in pem fuel cells". *Journal of Power Sources, 135*(1-2), pp. 95–109.

[18] Xing, X., Lum, K., Poh, H., and Wu, Y., 2010. "Optimization of assembly clamping pressure on performance of proton-exchange membrane fuel cells". *Journal of Power Sources, 195*, pp. 62–68.

[19] Karnik, A., Stefanopoulou, A., and Sun, J., 2007. "Water equilibria and management using a two-volume model of a polymer electrolyte fuel cell". *Journal of Power Sources, 164*.

[20] McKay, D., Siegel, J., Ott, W., and Stefanopoulou, A., 2008. "Parameterization and prediction of temporal fuel cell voltage behavior during flooding and drying conditions". *Journal of Power Sources, 178*.